Phonon confinement effects in ultrathin epitaxial bismuth films on silicon studied by time-resolved electron diffraction

B. Krenzer,[1] A. Hanisch-Blicharski,[1,*] P. Schneider,[1] Th. Payer,[1] S. Möllenbeck,[1] O. Osmani,[1] M. Kammler,[1] R. Meyer,[2] and M. Horn-von Hoegen[1]

[1] *Department of Physics, Center for Nanointegration (CeNIDE), University of Duisburg–Essen, Lotharstrasse 1, 47048 Duisburg, Germany*

[2] *Department of Mathematics and Computer Science, Laurentian University, 935 Ramsey Lake Road, Sudbury, Ontario, Canada P3E 2C6*

(Received 31 March 2009; revised manuscript received 19 May 2009; published 22 July 2009)

The transient temperature evolution of ultrathin bismuth films, epitaxially grown on a silicon single crystal, upon femtosecond laser excitation is studied by time-resolved electron diffraction. The exponential decay of the film temperature is explained by phonon reflection at the interface, which results in a strongly reduced thermal conduction in the cross plane of the layered system. The thermal boundary conductance is found to be as low as 1273 W/(K cm^2). Model calculations, including phonon confinement effects, explain the linear relationship between the observed film-temperature decay constant and the film thickness. Even for 2.5 nm thin films the phonon transmission probability across the interface is given by bulk properties. Our simulations show that phonon confinement effects are negligible for bismuth-film thicknesses larger than 1 nm.

DOI: 10.1103/PhysRevB.80.024307 PACS number(s): 44.10.+i, 61.05.jh, 63.22.−m, 68.35.−p

I. INTRODUCTION

Nowadays the physical properties of devices on the length scale of only a few nanometers become more and more important.[1–3] The interesting and often surprising physical properties of such small devices can basically be classified by two types of effects: an increased surface- or interface-to-volume ratio and confinement of particles and quasiparticles, such as electrons and phonons. An understanding of these effects is of utmost importance and can be potentially used to engineer the physical properties, e.g., the thermal and electrical conductivities of such nanobased devices.[4–8]

In the past it has been shown, that the reduction in one spatial dimension in thin films leads to an electron confinement forming quantum-well states.[9–16] Such a confinement is also expected for the vibrational degrees of freedom in a solid, i.e., phonons.[17–22] But only a few experimental investigations have dealt with the direct measurement of confined phonons.[23–28] Phonon confinement effects, which result in a reduction in the phonon group velocity and a change in the density of states, manifest themselves in a further reduction in the in-plane thermal conductivity.[18,29] This adds to the reduction in the thermal conductivity due to an increased phonon scattering at the surface and interface. Furthermore, confinement of electrons and phonons strongly alter the electron-phonon coupling in such nanoscale devices as compared to the bulk.[30–32]

Consequently, confinement effects should also influence the heat transport across the interface between two distinct materials.[33] The heat flow across an interface between a thin film and a substrate is drastically reduced compared to bulk diffusion and the temperature decay in the film is given by

$$cd\frac{\partial T_f(t)}{\partial t} = -\sigma_K[T_f(t) - T_s(t)], \tag{1}$$

with c as specific-heat capacity, d the film thickness, and σ_K the thermal boundary conductance.[4,34,35] T_f and T_s are the film and substrate temperatures, respectively. The above equation relates the thin-film temperature to the temperature difference at the interface. The thermal boundary conductance σ_K is related to the phonon-transmission probability t across the interface by[4,34–36]

$$\sigma_K = \frac{1}{2}\int_0^\infty c(\omega,T)\langle v(\omega)\rangle\langle t(\omega)\rangle d\omega, \tag{2}$$

where $\langle t(\omega)\rangle$ is the averaged phonon-transmission probability if multiple phonon modes contribute to the heat transport. $\langle v(\omega)\rangle$ is the averaged phonon group velocity perpendicular to the interface. $c(\omega,T)$ is the specific-heat capacity of phonons with energy $\hbar\omega$ at a temperature T.

Phonon confinement effects act on the phonon group velocity and thus on $\langle v(\omega)\rangle$.[18,29] In addition, the phonon-transmission probability will change with decreasing dimensions. For the determination of the phonon-transmission probability the two basic models are the acoustic mismatch model (AMM) and the diffuse mismatch model (DMM).[34,35] For their applicability two regimes are distinguished.[37] If the dominant phonon wavelength is larger than the interface roughness, the phonons are treated as elastic waves that are reflected and refracted at the interface. The ratio of the energy between the refracted wave compared to the incoming wave yields the transmission probability.[34,35,38] It turns out that a critical cone of total reflection evolves if the film material is acoustically thicker than the substrate. This is the case for phonon transport from a bismuth film into a silicon substrate. Phonons incident to the interface with angles larger than the critical angle, given by Snells law, are totally reflected at the interface. A change in the group velocity directly affects this critical angle. A decreasing group velocity with decreasing film thickness results in a narrower cone of total reflection, reducing the phonon-transmission probability.

 ©2009 The American Physical Society

In the case where the dominant phonon wavelength is smaller than the interface roughness, strong phonon scattering at the interface is assumed.[34,35,37] The probability in which state, i.e., film or substrate, the phonon is scattered only depends on the density of phonon states.[34,35] Again, phonon confinement results in changes in the density of states and thus the transmission probability.

Assuming energy independence, the transmission probabilities and group velocities in Eq. (2) are being substituted by

$$\langle v(\omega)\rangle \rightarrow \langle v(d)\rangle, \quad \langle t(\omega)\rangle \rightarrow \langle t(d)\rangle \tag{3}$$

and the thermal boundary conductance depends on the film thickness d

$$\sigma_{\mathrm{K}} = \sigma_{\mathrm{K}}(d) = \langle v(d)\rangle\langle t(d)\rangle \frac{1}{2}\int_0^\infty c(\omega,T)d\omega. \tag{4}$$

From Eq. (1) the decay constant of the film-temperature evolution is given by

$$\tau_{\mathrm{dec}} = \frac{c}{\sigma_{\mathrm{K}}(d)}d. \tag{5}$$

By determining the decay constant for different film thicknesses d, a deviation from a linear behavior between τ and d is indicative for phonon confinement in thin films. In a previous study we investigated the thickness dependence of the decay constant τ for Bi films on a Si(001) substrate down to 6 nm thickness, which corresponds to about 16 bilayers (bilayerheight is 0.394 nm).[39] No deviation from a linear relationship between τ and the film thickness d has been observed, suggesting that phonon confinement has a negligible influence on the heat transport across the interface.

It is noted, the temperature independence of the thermal boundary conductance σ_{K}, in the temperature range used in this study, is taken into account.[40] This results in a single exponential decay characterized by the decay constant τ_{dec} [Eq. (5)]. We previously verified experimentally that τ_{dec} is independent of the temperature.[39]

In this paper we present results of ultrathin Bi films down to 2.5 nm thickness, i.e., 6 bilayer height. In order to create such thin films, bismuth is deposited onto a Si(111) surface which has been shown in the past to result in extremely smooth, continuous, and well-defined films.[41–44] The Bi film is laterally only slightly compressed by 1.3% and the interface is abrupt and atomically flat.[43,44] Additionally, the films are grown under cleanest conditions and in a controlled fashion. This ensures the reduction in unknown parameters of the film morphology and the interface structure to a minimum.

II. EXPERIMENTAL

Prior to Bi deposition the Si sample (width=3.5 mm) was flashed to 1500 K and slowly cooled down resulting in a well-ordered (7×7)-reconstructed (111) surface. Bi films with film thicknesses below 6 nm were prepared by depositing Bi (99.9999%, MaTeK) from a Knudsen cell[45] onto Si(111) at 150 K. The film thickness was determined by a quartz microbalance, which was calibrated by *ex situ* non-contact atomic force microscopy (NC-AFM) and x-ray reflectometry. After deposition, the films were annealed to 420 K and subsequently held at 400 K for 10 min. This recipe was found to result in flat films.[41,42] The thinnest film prepared with this method was 2.5 nm. Figure 1 shows a NC-AFM image and a low-energy electron diffraction (LEED) of a 2.5 nm thin Bi film.

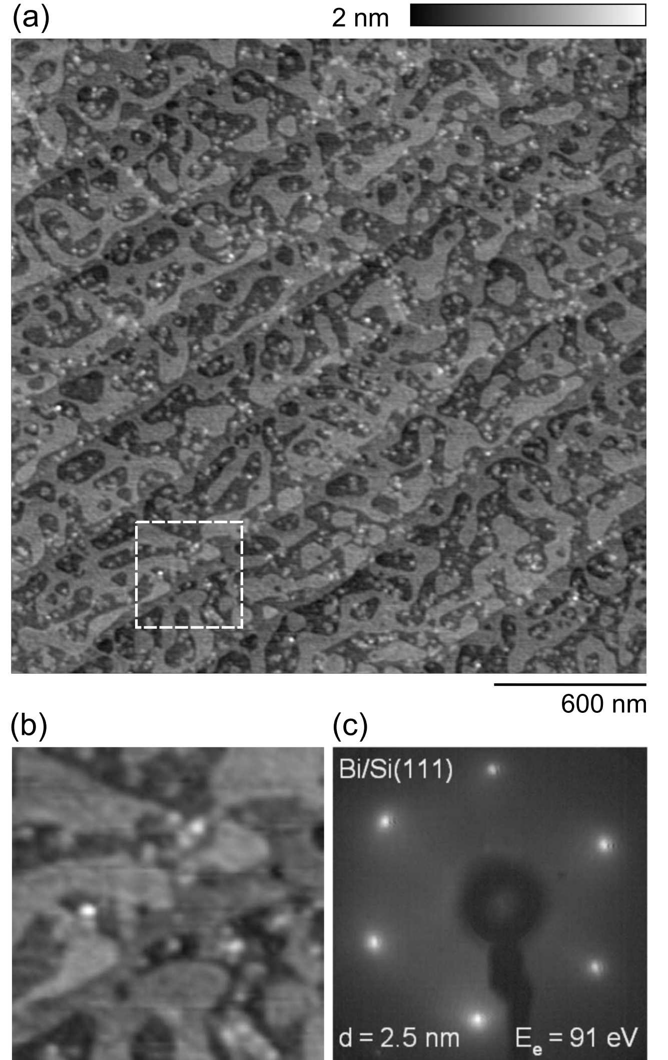

FIG. 1. (a) NC-AFM image of a 2.5 nm thin Bi film on Si(111). The film was grown at 150 K and annealed to 420 K and subsequently held at 400 K for 10 min. The scanning range of the image is 2.5 μm×2.5 μm. Steps of the underlying Si(111) substrate are clearly visible. The marked area (dashed square) is displayed in (b) with a magnification factor of 3. The step height between two adjacent terraces is one bilayer, i.e., 3.94 Å. (c) LEED pattern of the 2.5 nm thin Bi film. As evident from the hexagonal symmetry the Bi film is (111) oriented.

In the NC-AFM image shown in Fig. 1(a) large smooth areas are observed which are separated from each other by a bilayer height step [see Fig. 1(b)]. Additionally, steps from the underlying Si substrate are observed. We conclude that such prepared films are single crystalline, continuous, well ordered, and smooth as previously observed.[41–44] As evident from the hexagonal symmetry of the LEED pattern the Bi

film is (111) oriented [Fig. 1(c)]. Films with larger thicknesses were prepared by subsequent deposition of additional Bi at 400 K onto a 6-nm-thick base film, which was prepared following the above described recipe. These films are also well ordered and smooth (not shown here). The morphology of the films remained unchanged even after several hours of laser bombardment, as verified by LEED.

The thermal boundary conductance was determined by means of ultrafast electron diffraction. In this pump-probe technique a short electron pulse is scattered at the surface at different delays from an initial laser pump pulse.[46–51] The pump pulse (photon energy 1.55 eV, wavelength 800 nm) are ~50 fs short laser pulses at a repetition rate of 5 kHz. For all experiments the laser fluence on the sample was set to $Q_A = 2.3$ mJ/cm^2. A small fraction (~20%) of the initial pulses is frequency tripled and directed onto a thin gold film. Via photoemission short electron pulses are created.[50] The electron pulses are accelerated to 7 keV energy and scattered at the sample at 5° angle of incidence which ensures surface sensitivity [reflection high-energy electron-diffraction (RHEED) geometry]. The resulting perpendicular momentum transfer is $\Delta k_\perp = 7.5$ Å^{-1}. The electron-diffraction pattern is intensified using a multichannel plate detector and recorded by a cooled charged-coupled-device camera.[50] From the temporal evolution of the diffraction spot intensity the transient surface temperature is derived using the Debye-Waller effect.[47,50–52] Because the excited area (2×3 mm^2) is on the order than the probed area (0.4×3.5 mm^2) the lateral heat diffusion can be neglected and the temperature decay is given by the heat transport in the direction perpendicular to the interface (cross plane). In the thin Bi films a homogeneous temperature distribution in the cross plane is established after ~6 ps and the decay of the transient surface temperature displays the temperature decay of the whole film.[53]

III. RESULTS AND DISCUSSION

The transient surface temperature of the 2.5 nm thin Bi film is shown in Fig. 2. The inset shows a RHEED pattern at negative delays, i.e., the probe pulse arrives at the surface before the pump pulse. The indicated diffraction spot was used to extract the transient surface temperature shown in Fig. 2. Analyzing the other diffraction spots result in similar transient temperature evolutions especially in the same decay constant τ_{dec}.

For negative delays the surface has a constant temperature of 90 K, which is the base temperature for all experiments in this study. Around zero delay the surface temperature increases steeply to a maximum temperature of almost 210 K. Subsequently, the surface cools down exponentially to the base temperature. The observed temperature evolution can be described with the phenomenological function[54,55]

$$T(t) = \Theta(t)\Delta T(1 - e^{-t/\tau_{\mathrm{inc}}})e^{-t/\tau_{\mathrm{dec}}} + T_0. \quad (6)$$

$\Theta(t)$ is the Heaviside step function, ΔT is the initial temperature increase, and T_0 is the base temperature. The time constant τ_{inc} is the rising time constant which is given by the temporal resolution of the experimental setup.[39] The decay constant τ_{dec} is equal to the decay constant from Eq. (5). The fit of Eq. (6) to the experimental data yields $\Delta T = (157\pm 8)$ K, $\tau_{\mathrm{inc}} = (41\pm 4)$ ps, and $\tau_{\mathrm{dec}} = (243\pm 15)$ ps (cf. Fig. 2).

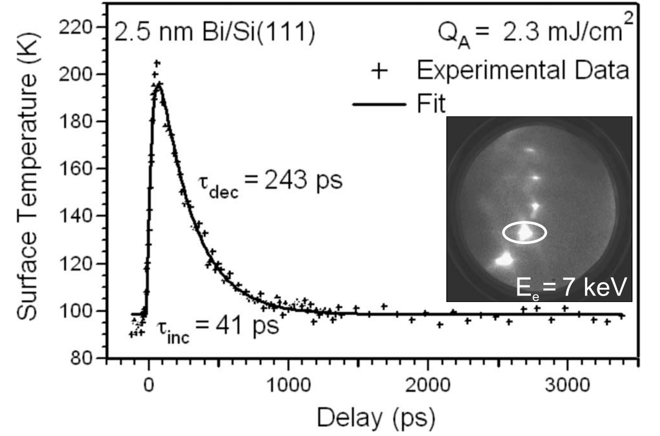

FIG. 2. Transient surface temperature of a 2.5 nm thin Bi film. The laser fluence is $Q_A = 2.3$ mJ/cm^2. The experimental data are shown as markers. The solid line is a fit of Eq. (6). The fit yields a temperature jump of (157 ± 8) K, a time constant for the increase of $\tau_{\mathrm{inc}} = (41\pm 4)$ ps, and a decay constant of $\tau_{\mathrm{dec}} = (243\pm 15)$ ps. The inset shows the RHEED pattern at a negative delay, i.e., excitation occurs after scattering of the electron probe pulse. The indicated diffraction spot was used to extract the transient temperature evolution.

The transient temperature evolutions for a series of film thicknesses between 2.5 and 34.5 nm are shown in Fig. 3(a). For better comparability the transient temperature evolutions are normalized such as $\{[T(t)-T_0]/(T_{\mathrm{max}}-T_0)\}$, with T_0 the base temperature and T_{max} the maximum temperature at zero delay. $T(t)$ is determined as described above. With increasing thickness a slower film cooling is observed. The decay constant τ_{dec} for the different film thicknesses which are obtained from the fit of Eq. (6) to the experimental data and shown in Figs. 3(b) and 3(c). As evident from Figs. 3(b) and 3(c) the decay constant linearly depends on the film thickness down to thicknesses as small as 2.5 nm. This thickness corresponds to 6–7 atomic bismuth bilayers. A linear fit to the experimental data yields a slope of (93.5 ± 1.2) ps/nm. By using Eq. (5) this yields a thermal boundary conductance $\sigma_K = (1273\pm 16)$ W/(K cm^2) (cf. Table I for the specific-heat c). This value is in very good agreement to the thermal boundary conductance of the Bi and Si(001) interface, which was found to be $\sigma_K = (1320\pm 60)$ W/(K cm^2).[39]

The independence of the thermal boundary conductance σ_K from the orientation of the substrate suggests that the detailed nature of the interface only plays minor role. Additionally, the value of σ_K is in accordance to the calculated values, using the AMM and DMM for the determination of the phonon transmission probability.[51] We conclude that the coupling of electrons to the image potential states proposed previously[56] has a minor contribution to the energy transport across the interface and can be neglected.

From these findings it is not possible to distinguish between the microscopic processes of energy transfer at the interface, i.e., strong scattering (DMM) or refraction of elas-

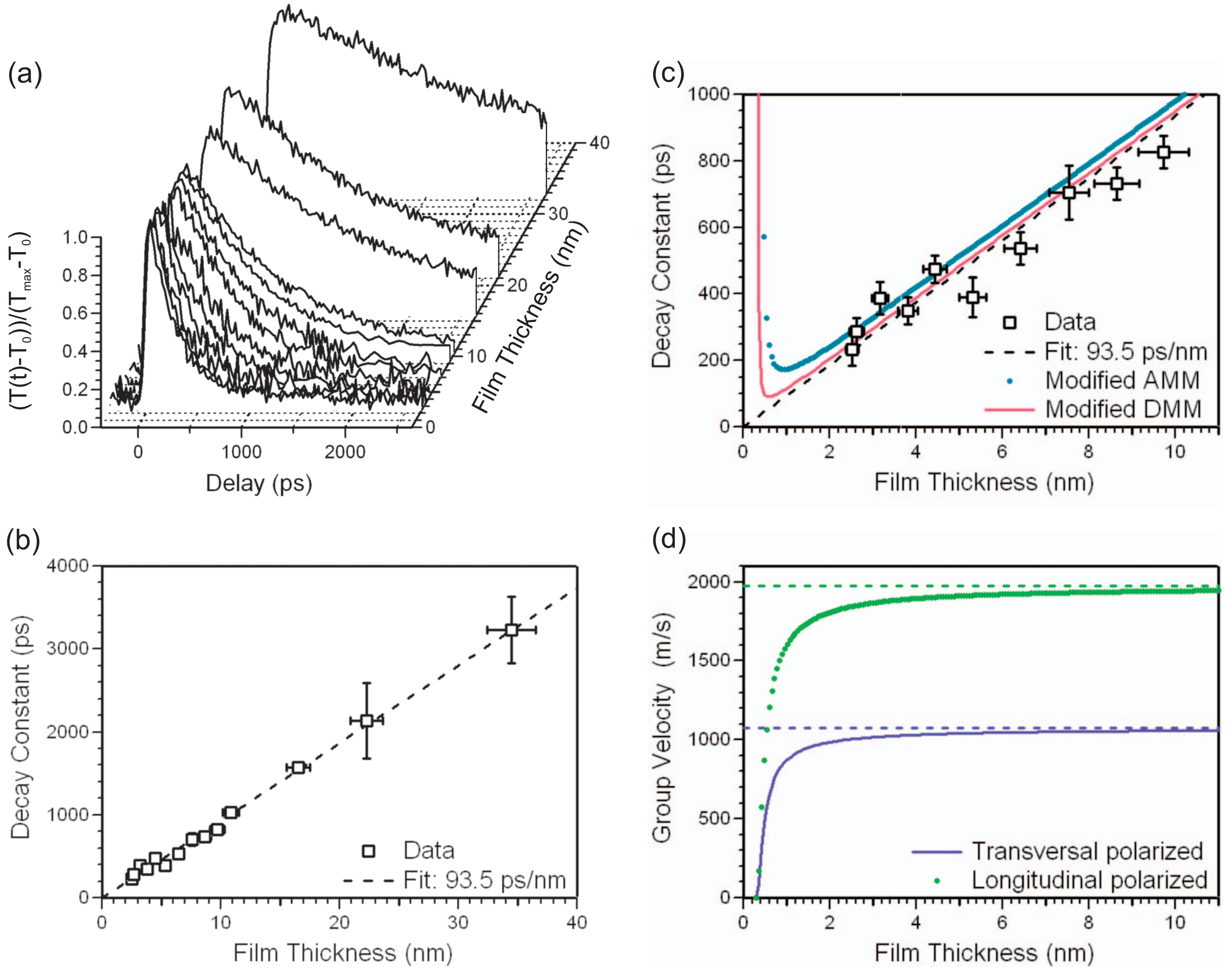

FIG. 3. (Color) (a) Normalized transient temperature evolutions $\{[T(t)-T_0]/(T_{\max}-T_0)\}$ for different film thicknesses. The base temperature $T_0=90$ K was the same for all experiment. $T_{\max}$ is the maximum temperature at zero delay. The pump fluence for all experiments was $Q_A=2.3$ mJ/cm^2. (b) Thickness dependence of the decay constant τ_{dec}. (c) Close-up view of the thickness range between 0 and 11 nm. The dashed line in (b) and (c) is a line fit to the experimental data yielding a slope of (93.5 ± 1.2) ps/nm. In (c) the results of model calculations for the decay constant using the AMM (dots) and the DMM (solid line) for the determination of the phonon transmission coefficient are additionally displayed (modified AMM/DMM, see text for details). (d) Thickness dependence of the phonon group velocity for the transversal and longitudinal polarized phonons which is used in the model calculations. The horizontal lines are the respective group velocities for bulk Bi.

tic waves at a smooth interface (AMM). However, phonon confinement effects were not considered so far.

As stated in Sec. I a size reduction in one or more dimension of a system is reflected in a change in the phonon group velocity v and density of states.[18,33] The decay constant [Eq. (5)] can be written as

$$\tau_{\text{dec}}=\frac{\langle v(\infty)\rangle\langle t(\infty)\rangle}{\langle v(d)\rangle\langle t(d)\rangle}\cdot\frac{c}{\sigma_{\text{K}}(\infty)}d, \quad (7)$$

with $\sigma_{\text{K}}(\infty)$, $\langle v(\infty)\rangle$, and $\langle t(\infty)\rangle$ the values for the thermal boundary conductance, averaged group velocity, and the averaged transmission probability for thick films with bulk properties. $\langle v(d)\rangle$ and $\langle t(d)\rangle$ are the averaged group velocity and transmission probability for a given film thickness d.

For bismuth the group velocity $v(d)$ is determined by[33,57]

$$v(d)=v_\infty \exp\left[-\frac{(H_{\text{m}}/T_{\text{m}}-R)}{3R(d/d_0-1)}\right], \quad (8)$$

with H_{m} the melting enthalpy, T_{m} melting temperature, and R the ideal-gas constant. The critical size d_0 is defined by the size of the particle or the thickness of a film when all atoms are located at the surface. For a thin film on a substrate the critical size is given by $d_0=2r_a$, with r_a the atomic radius, which is taken as the covalent radius in this study. The results of Eq. (8) using the literature values from Table I are shown in Fig. 3(d). The group velocities vanish for film thicknesses approaching the critical thickness d_0, increase

exponentially with increasing film thickness, and asymptotically reach the bulk values.

Using these phonon group velocities, the phonon transmission probability $\alpha(\theta,d)$ depending on the incident angle on the interface θ are obtained by applying the acoustic equivalents of the Fresnel equations in optics (cf. Table I for the material parameters).[38] It is noted that mode conversion is included in the calculation, e.g., longitudinal polarized phonons in Bi are converted to transversal polarized phonons in the Si substrate. From Fig. 3(d) it is also concluded that with decreasing Bi-film thickness, which results in smaller phonon group velocities, the cone of total reflection gets narrower. To be specific, in this AMM framework the change in the phonon transmission probability is caused by the reduction in the group velocity. The average of the angle-integrated transmission probabilities $\alpha(\theta,d)$ is used as $\langle t(d)\rangle$ in Eq. (7) for the determination of the decay constant τ_{dec}.

A discrete nature of the phonon density of states has also a direct impact on the transmission probability calculated in the framework of the diffuse mismatch model. In order to get insight into the thickness dependence of the density of states we performed molecular-dynamics simulations. In these calculations, the atoms of the two components, i.e., bismuth and silicon, were described by Lennard-Jones potentials. The pair interactions were truncated and shifted to zero beyond the fourth neighbor shell. For the masses of the two components, the experimental values of Bi and Si were taken and the energy parameters of the pair interaction were chosen in order to obtain maximum phonon frequencies of 2 and 20 THz, respectively. For the mixed interaction, the arithmetic average of the energy parameters of both components has been used. Finally, a single length-scale parameter that results in the correct nearest-neighbor distance for Si at $T=0$ K was applied to both components.

The initial configurations for the molecular-dynamics simulations consisted of a stack of close-packed planes with an fcc-like stacking sequence. The individual planes were nearly quadratic with a side length of approximately 10.6 nm and contain 2340 atoms, each. All configurations were made with a substrate of 100 Si-like layers. On top of the substrate, films with $N=1$, 2, 4, 8, 16, 32, and 48 layers of Bi-like atoms were placed. Periodic boundary conditions were applied in the x and y directions, only. After a careful equilibration at $T=77$ K, simulation runs over a period of 25 ps

TABLE I. Bulk values for the specific-heat capacity c, density ρ, bulk group velocities of the transversal v_t and longitudinal v_l polarized phonons, melting enthalpy H_{m}, melting temperature T_{m}, and covalent atomic radius r_a (Refs. 58–61).

	Bi	Si
c [10^6 J/(K m^3)]	1.19	1.66
ρ (kg/m^3)	9800	2330
v_t (m/s)	1074	5845
v_l (m/s)	1972	8433
H_{m} [kJ/(K mol)]	11.30	50.25
T_{m} (K)	544	1687
r_a (nm)	0.148	0.111

(12 500 simulation steps) were performed and the vibrational density of states (VDOS) was derived with the help of the velocity-autocorrelation function. The final VDOS of each configuration was obtained from averages over 5–40 of such simulation runs, depending on the number of Bi layers. All extracted VDOS were normalized such that the integral yields unity.

It should be noted that the model described in the preceding paragraphs is certainly not a realistic model of the experimental system studied in this work. In particular, the use of Lennard-Jones potentials is neither able to describe the crystal structure of Bi and Si, nor does it reproduce the optical-phonon parts in the two materials. However, the energies of the optical phonons in silicon are much larger than any phonon energy in bismuth.[62,63] Only the low-energy part of the acoustic phonons in silicon is important. Because of their small group velocity the optical phonons in Bi negligibly contribute to the overall heat transport across the interface [cf. Eq. (2)]. The model we use, however, does reflect two important properties of the experimental system: the big differences in the atomic masses and the discrepancy of the phonon frequencies of both components, which is shown in Fig. 4(a).

Figure 4(a) shows the normalized partial VDOS of the two components for the configuration containing 48 Bi-like layers which should behave like a bulk system. The figure shows that the phonon spectra of both model components are indeed clearly separated with almost no overlap. The small peak at 11 meV in the partial VDOS of Bi is due to the interface between film and substrate. The small overlap between the vibrational density of states of Bi and Si is the reason for the small thermal boundary conductance.

The evolution of the partial density of states in the Bi slab with decreasing film thickness is shown in Fig. 4(b). For films with thicknesses of 16 or more layers, the figure shows only minor differences in the VDOS. Even for the eight-layer film, the differences are rather limited and, in particular, the low-energy part below 3 meV is nearly unchanged. Only for film thicknesses of four or less layers the finite thickness of the film becomes apparent in the vibrational density of states. The fact, that the VDOS of such thin films is almost identical to bulk matter has also been found previously for spherical clusters with a diameter of 2.5 nm.[64] It is concluded that the transmission probability $t(d)$ for phonons of thin films is unchanged and the same as for bulklike films. It is noted, that an additional thickness dependence of the decay constant [Eq. (7)] is introduced by the group velocities.

The results of Eq. (7) using the thickness-dependent group velocities and transmission probabilities are shown in Fig. 3(c), indicated as modified AMM and DMM. For the thermal boundary conductance of the thick Bi film $\sigma_{\mathrm{K}}(\infty)$ the experimentally determined value of 1273 W/(K cm^2) was used. The averaged phonon group velocity is $\langle v(\infty)\rangle=1373$ m/s (cf. Table I). In the AMM the phonon transmission probability for the longitudinal-polarized phonons is 0.0223 and the two transversal-polarized phonons are 0.005 and 0.008, respectively.[51] This results in an averaged phonon transmission probability $\langle t(\infty)\rangle=0.0118$ which is used in Eq. (7).

For film thicknesses approaching the critical size d_0, the decay constant τ_{dec} diverges because the group velocity is

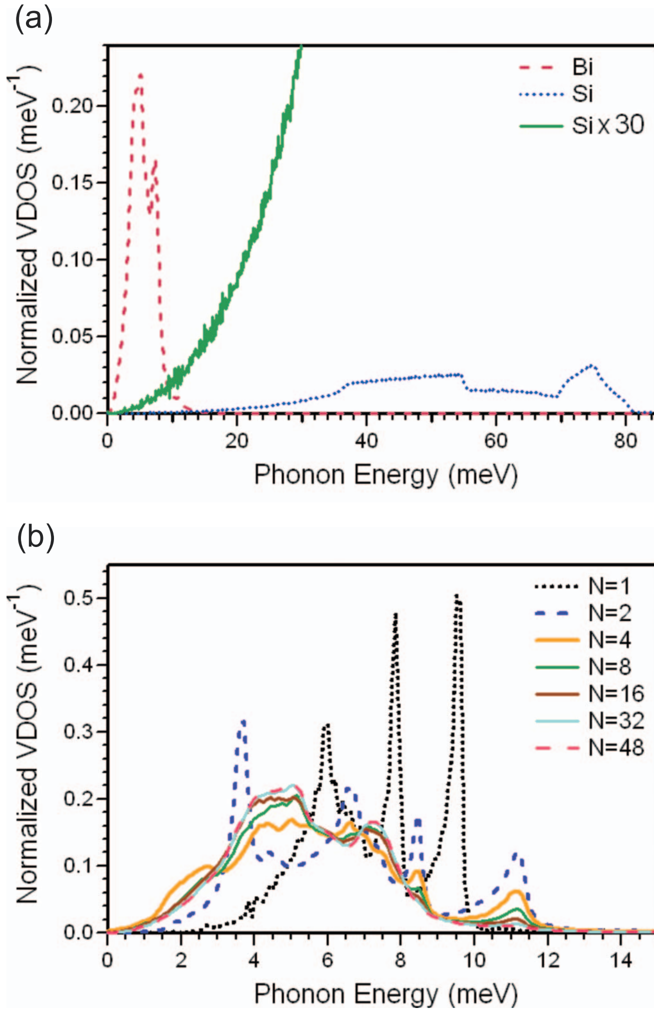

FIG. 4. (Color) (a) Partial VDOS of the system containing 48 Bi-like (red) and 100 Si-like (blue) layers. The acoustic part of the Si-like slab is additionally displayed with a magnification of 30 (green). (b) Partial VDOS of $N=1,2,4,8,16,32,48$ Bi-like layers on 100 Si-like layers. All VDOS are normalized so that the integral over the energy results in unity. The VDOS of the $N=32$ and $N=48$ Bi-like layers in (b) are identical.

vanishing [cf. Fig. 3(d)]. For increasing film thicknesses the decay constant asymptotically reaches the linear behavior expected from Eq. (5). It is evident from Fig. 3(c) that the experimental data are well described by the above models. Only for film thicknesses smaller than 1 nm, corresponding to less than three Bi bilayers, a deviation from a linear relationship can be expected. For the thickness range larger than the measured 2.5 nm, phonon confinement effects only play a minor role and can be neglected for the investigated Bi/Si system. In addition, both models, AMM and DMM including phonon confinement effects, are capable of describing the phonon transmission probability and thus the heat transport from thin Bi films into a Si substrate. This finding is in contrast to previous results for the transmission probability in nanolaminates, where phonon confinement effects drastically reduce the thermal conductivity.[33,65]

IV. CONCLUSIONS

We have investigated the heat transport from laser-heated thin Bi films into a (111)-oriented Si substrate by means of ultrafast electron diffraction. From the linear relationship between the film-temperature decay constant and the film thickness a thermal boundary conductance of (1273 ± 16) W/(K cm^2) has been determined. This value is the same as for a Bi/Si(001) system suggesting that the detailed nature of the interface has a negligible effect on the thermal boundary conductance. No deviation from a linear relationship between the decay constant and the film thickness is observed. This result supports that phonon confinement effects are negligible for the Bi/Si heterosystem and Bi-film thicknesses larger than 2.5 nm. We performed simulations for the thickness dependence of the decay constant using the acoustic and diffuse mismatch model including phonon confinement effects, i.e., reduction in the phonon group velocity and phonon density of states. We find that the phonon density of states is bulklike for films with more than eight layers, which results in a film-thickness-independent phonon transmission probability in the framework of the DMM. In the AMM, thickness-dependent phonon group velocities, however, result in smaller cones of total reflection reducing the phonon transmission probability. However, the such modeled dependence of the decay constant is in very good agreement to the experimental results. For Bi/Si, phonon confinement becomes important only for film thicknesses below 1 nm.

ACKNOWLEDGMENTS

The authors thank M. Vennemann for the x-ray reflectrometry measurements and P. Zhou and M. Ligges for technical support. The model calculations were carried out on the facilities of the Shared Hierarchical Academic Research Computing Network (SHARCNET). This work was funded by the Deutsche Forschungsgemeinschaft through SFB 616 "energy dissipation at surfaces," which is gratefully acknowledged.

*anja.hanisch@uni-due.de

[1] R. Venkatasubramanian, E. Siivola, T. Colpitts, and B. O'Quinn, Nature (London) **413**, 597 (2001).
[2] A. Balandin and K. L. Wang, J. Appl. Phys. **84**, 6149 (1998).
[3] L. D. Hicks and M. S. Dresselhaus, Phys. Rev. B **47**, 12727 (1993).
[4] D. G. Cahill, W. K. Ford, K. E. Goodson, G. D. Mahan, A. Majumdar, H. J. Maris, R. Merlin, and S. R. Phillpot, J. Appl. Phys. **93**, 793 (2003).
[5] D. L. Nika, E. P. Pokatilov, and A. A. Balandin, Appl. Phys. Lett. **93**, 173111 (2008).
[6] L. Aballe, A. Barinov, A. Locatelli, S. Heun, and M. Kiskinova, Phys. Rev. Lett. **93**, 196103 (2004).
[7] Y. Guo, Y.-F. Zhang, X.-Y. Bao, T.-Z. Han, Z. Tang, L.-X.

Zhang, W.-G. Zhu, E. G. Wang, Q. Niu, Z. Q. Qiu, Jin-Feng Jia, Zhong-Xian Zhao, and Qi-Kun Xue, Science **306**, 1915 (2004).
[8] G. Chen, A. Narayanaswamy, and C. Dames, Superlattices Microstruct. **35**, 161 (2004).
[9] J. J. Paggel, T. Miller, and T.-C. Chiang, Science **283**, 1709 (1999).
[10] N. Miyata, K. Horikoshi, T. Hirahara, S. Hasegawa, C. M. Wei, and I. Matsuda, Phys. Rev. B **78**, 245405 (2008).
[11] S.-J. Tang, W.-K. Chang, Y.-M. Chiu, H.-Y. Chen, C.-M. Cheng, K.-D. Tsuei, T. Miller, and T.-C. Chiang, Phys. Rev. B **78**, 245407 (2008).
[12] L. Aballe, C. Rogero, S. Gokhale, S. Kulkarni, and K. Horn, Surf. Sci. **482-485**, 488 (2001).
[13] L. Aballe, C. Rogero, P. Kratzer, S. Gokhale, and K. Horn, Phys. Rev. Lett. **87**, 156801 (2001).
[14] J. H. Dil, J. W. Kim, T. Kampen, K. Horn, and A. R. H. F. Ettema, Phys. Rev. B **73**, 161308(R) (2006).
[15] T. Hirahara, T. Nagao, I. Matsuda, G. Bihlmayer, E. V. Chulkov, Y. M. Koroteev, P. M. Echenique, M. Saito, and S. Hasegawa, Phys. Rev. Lett. **97**, 146803 (2006).
[16] T. Hirahara, K. Miyamoto, A. Kimura, Y. Niinuma, G. Bihlmayer, E. V. Chulkov, T. Nagao, I. Matsuda, S. Qiao, K. Shimada, H. Namatame, M. Taniguchi, and S. Hasegawa, New J. Phys. **10**, 083038 (2008).
[17] A. Melikyan and H. Minassian, Chem. Phys. Lett. **331**, 115 (2000).
[18] A. Balandin and K. L. Wang, Phys. Rev. B **58**, 1544 (1998).
[19] J. Zou and A. Balandin, J. Appl. Phys. **89**, 2932 (2001).
[20] E. H. Hwang, S. Das Sarma, and M. A. Stroscio, Phys. Rev. B **61**, 8659 (2000).
[21] P. Heino, Microsyst. Technol. **15**, 75 (2009).
[22] X. Lü, J. Appl. Phys. **104**, 054314 (2008).
[23] A. Balandin, A. Khitun, J. L. Liu, K. L. Wang, T. Borca-Tasciuc, and G. Chen, 18th International Conference on Theromelectrics, 1999 (unpublished), p. 189.
[24] A. M. de Paula, L. C. Barbosa, C. H. B. Cruz, O. L. Alves, and J. A. Sanjurjo, Appl. Phys. Lett. **69**, 357 (1996).
[25] D. Bersani, P. P. Lottici, and X.-Z. Ding, Appl. Phys. Lett. **72**, 73 (1998).
[26] J. Hone, B. Batlogg, Z. Benes, A. T. Johnson, and J. E. Fischer, Science **289**, 1730 (2000).
[27] B. Roldan Cuenya, A. Naitabdi, J. Croy, W. Sturhahn, J. Y. Zhao, E. E. Alp, R. Meyer, D. Sudfeld, E. Schuster, and W. Keune, Phys. Rev. B **76**, 195422 (2007).
[28] B. Roldan Cuenya, W. Keune, R. Peters, E. Schuster, B. Sahoo, U. von Hörsten, W. Sturhahn, J. Zhao, T. S. Toellner, E. E. Alp, and S. D. Bader, Phys. Rev. B **77**, 165410 (2008).
[29] G. Chen, C. L. Tien, and J. Thermo, J. Thermophys. Heat Transfer **7**, 311 (1993).
[30] B. K. Ridley, Rep. Prog. Phys. **54**, 169 (1991).
[31] N. Bannov, V. Aristov, V. Mitin, and M. A. Stroscio, Phys. Rev. B **51**, 9930 (1995).
[32] P. S. Kirchmann and U. Bovensiepen, Phys. Rev. B **78**, 035437 (2008).
[33] L. H. Liang, Y. G. Wei, and B. Li, J. Appl. Phys. **103**, 084314 (2008).
[34] E. T. Swartz and R. O. Pohl, Rev. Mod. Phys. **61**, 605 (1989).
[35] R. J. Stoner and H. J. Maris, Phys. Rev. B **48**, 16373 (1993).
[36] D. A. Young and H. J. Maris, Phys. Rev. B **40**, 3685 (1989).
[37] P. E. Phelan, ASME J. Heat Transfer **120**, 37 (1998).
[38] J. Miklowitz, *The Theory of Elastic Waves and Waveguides*, Applied Mathematics and Mechanics Vol. 22 (North-Holland, Amsterdam, 1978).
[39] A. Hanisch, B. Krenzer, T. Pelka, S. Möllenbeck, and M. Horn-von Hoegen, Phys. Rev. B **77**, 125410 (2008).
[40] J. Wang and J.-S. Wang, J. Phys.: Condens. Matter **19**, 236211 (2007).
[41] S. Yaginuma, T. Nagao, J. T. Sadowski, A. Pucci, Y. Fujikawa, and T. Sakurai, Surf. Sci. **547**, L877 (2003).
[42] T. Nagao, J. T. Sadowski, M. Saito, S. Yaginuma, Y. Fujikawa, T. Kogure, T. Ohno, Y. Hasegawa, S. Hasegawa, and T. Sakurai, Phys. Rev. Lett. **93**, 105501 (2004).
[43] T. Nagao, S. Yaginuma, M. Saito, T. Kogure, J. T. Sadowski, T. Ohno, S. Hasegawa, and T. Sakurai, Surf. Sci. **590**, L247 (2005).
[44] M. Kammler and M. Horn-von Hoegen, Surf. Sci. **576**, 56 (2005).
[45] P. Kury, R. Hild, D. Thien, H.-L. Günter, F.-J. Meyer zu Heringdorf, and M. Horn-von Hoegen, Rev. Sci. Instrum. **76**, 083906 (2005).
[46] E. A. Murphy, H. E. Elsayed-Ali, and J. W. Herman, Phys. Rev. B **48**, 4921 (1993).
[47] H. E. Elsayed-Ali and J. W. Herman, Appl. Phys. Lett. **57**, 1508 (1990).
[48] C.-Y. Ruan, F. Vigliotti, V. A. Lobastov, S. Chen, and A. H. Zewail, Proc. Natl. Acad. Sci. U.S.A. **101**, 1123 (2004).
[49] D.-S. Yang, N. Gedik, and A. H. Zewail, J. Phys. Chem. C **111**, 4889 (2007).
[50] A. Janzen, B. Krenzer, O. Heinz, P. Zhou, D. Thien, A. Hanisch, F.-J. Meyer zu Heringdorf, D. von der Linde, and M. Horn-von Hoegen, Rev. Sci. Instrum. **78**, 013906 (2007).
[51] B. Krenzer, A. Janzen, P. Zhou, D. von der Linde, and M. Horn-von Hoegen, New J. Phys. **8**, 190 (2006).
[52] A. Janzen, B. Krenzer, P. Zhou, D. von der Linde, and M. Horn-von Hoegen, Surf. Sci. **600**, 4094 (2006).
[53] B. Krenzer, A. Hanisch, A. Duvenbeck, B. Rethfeld, and M. Horn-von Hoegen, J. Nanomater. **2008**, 590609 (2008).
[54] C.-K. Sun, F. Vallée, L. Acioli, E. P. Ippen, and J. G. Fujimoto, Phys. Rev. B **48**, 12365 (1993).
[55] L. Guidoni, E. Beaurepaire, and J.-Y. Bigot, Phys. Rev. Lett. **89**, 017401 (2002).
[56] G. D. Mahan, Phys. Rev. B **79**, 075408 (2009).
[57] Z. Zhang, M. Zhao, and Q. Jiang, Semicond. Sci. Technol. **16**, L33 (2001).
[58] W. Martienssen, *Springer Handbook of Condensed Matter and Materials Data* (Springer, Berlin, New York, 2005).
[59] B. Cordero, V. Gómez, A. E. Platero-Prats, M. Revés, J. Echeverría, E. Cremades, F. Barragán, and S. Alvarez, Dalton Trans. **2008**, 2832 (2008).
[60] Y. Eckstein, A. W. Lawson, and D. H. Reneker, J. Appl. Phys. **31**, 1534 (1960).
[61] H. J. McSkimin and P. Andreatch, J. Appl. Phys. **35**, 2161 (1964).
[62] W. Weber, Phys. Rev. B **15**, 4789 (1977).
[63] É. D. Murray, S. Fahy, D. Prendergast, T. Ogitsu, D. M. Fritz, and D. A. Reis, Phys. Rev. B **75**, 184301 (2007).
[64] R. Meyer, L. J. Lewis, S. Prakash, and P. Entel, Phys. Rev. B **68**, 104303 (2003).
[65] R. M. Costescu, D. G. Cahill, F. H. Fabreguette, Z. A. Sechrist, and S. M. George, Science **303**, 989 (2004).